10ème Congrès Français d'Acoustique

Lyon, 12-16 Avril 2010

PIV and POD Applied to High Amplitude Acoustic Flow at a Tube Termination

Robert Macdonald[1], David Skulina[1], Murray Campbell[1], Jean-Christophe Valiere[2], David Marx[2], Helene Bailliet[2]

[1] School of Physics and Astronomy, University of Edinburgh, Edinburgh EH9 3JZ, U.K.

[2] Institut PPRIME, CNRS, Université de Poitiers, UPR3346, ENSI Poitiers, Bât K, Campus Sud , 40 avenue du Recteur Pineau, 86022 POITIERS, France

At sound levels encountered in musical wind instruments the oscillating flow at the tube termination can produce periodic local non-linear flow effects. PIV is used to measure the complex flow at the termination of a model wind instrument for a range of sound levels and geometries. POD analysis is then applied to the velocity maps, and the ability of the technique to separate the acoustic flow from the induced non-linear flow is assessed. The percentage of kinetic energy in the upper POD modes is used to indicate the strength of the non-linear flow effects, which is found to be dependent on the Strouhal number of the flow. Acoustic streaming is also analysed from the PIV data. The ratio of streaming velocity to acoustic particle velocity is found to depend on the Strouhal number.

1 Introduction

When a sound wave of a sufficiently large amplitude travels past a sufficiently sharp discontinuity, local non-linear flow effects (vortices, free shear layers and jets) are generated which are superimposed onto the acoustic flow. Their effect can be measured as a loss of energy from the acoustic flow. Ingard and Labate [1] demonstrated that in the case of an orifice in a waveguide, the energy lost from the sound in the waveguide was equivalent to the energy of the non-linear flow effects generated in the region of the orifice.

Proper Orthogonal Decomposition (POD) is an analysis technique used, most commonly in the study of turbulent flows, to identify distinct flow structures. Marx et al [2] have recently suggested that it is possible to separate a purely acoustic flow from the non-linear flow induced by it using POD. They applied the technique to Particle Image Velocimetry (PIV) data of oscillating flow around a step inside a closed waveguide. It was found that POD could be used to pick out a motion that spatially resembled potential flow and varied as a sine wave in time, with the frequency of the loudspeaker excitation. This was identified with the purely acoustic motion. Other modes of the POD described the formation and development of vortices over the acoustic cycle. It was found that the amount of energy in the vortex formation modes relative to the acoustic mode was largely dictated by the Strouhal number of the flow.

In this paper the use of POD to study local non-linear effects created by an acoustic flow is extended to the case of a tube open at one end under resonance, using PIV data obtained by Skulina [3]. The experimental apparatus and procedure are briefly described in section 2. The principles of POD are then outlined in 3. The results of the POD analysis are presented in section 4. Section 4.1 considers how accurately POD can pick out the purely acoustic motion. Section 4.2 looks at how POD describes the non-linear flow effects. The energy transferred to local non-linear flow effects is analysed in section 4.3, which concludes with a discussion on the governing Strouhal number of the flow.

2 Experimental procedure

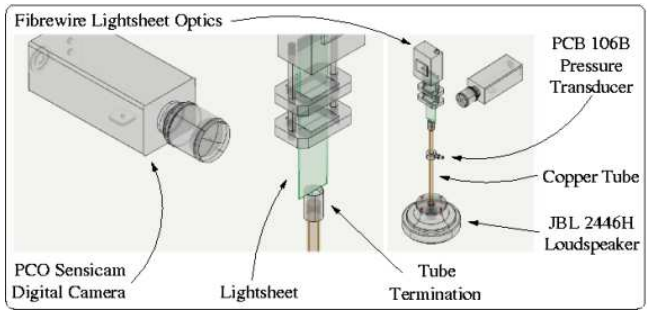

FIGURE 1 – Experimental apparatus for tube termination PIV experiments [3].

A diagram showing the main experimental apparatus used in the PIV experiments is given in figure 1. A copper tube of internal radius 8 mm and wall thickness 1 mm was coupled to a JBL 2446H 8Ω compression driver. Termination pieces with different geometries could be fitted to the open end. The geometry that was varied was the internal radius of curvature r at the open end. All terminations had a wall thickness of 4.5 mm. The terminations were constructed in aluminium and then anodised black to minimise reflective surfaces for use in PIV experiments. The length of the tube from the loudspeaker cavity to the open end of the termination was 460 mm. The system was excited at its fundamental resonant frequency of 380Hz frequency for the PIV measurements. A PCB Piezotronics model 106B pressure transducer was mounted into the copper tube 160 mm from the open end and was used to measure the sound pressure within the tube. From this, the RMS pressure at the pressure anti-node p_{an} (located roughly halfway along the tube) could be calculated.

An Oxford Lasers LS20-50 copper vapour laser with a minimum pulse separation time of 20μs was connected via an optical fibre to the light sheet delivery optics, producing a light sheet 50 mm wide and 1 mm thick at its narrowest point. The average power of the laser is 20 W and each light pulse has a duration of 30 ns at a wavelength of 510.6 nm (green). The light sheet was aligned with the tube axis and a PCO Sensicam 'Double Shutter' CCD camera positioned to view an area of interest in the seeded flow around the open end of the tube, perpendicular to the light sheet. This camera can take two separate images at a resolution of 1280×1024 pixels which are synchronised to the light pulses from the laser. Image pairs were acquired at intervals of approximately 0.5 s, synchronised to a specific phase of the acoustic cycle. 30 measurements were made at each of 10 different phase angles, so that averaging could be carried out during post-processing. Details of the PIV image acquisition and analysis are given in [3].

The RMS acoustic velocity at the velocity antinode (at the end of the tube) u_{an} can be approximated by assuming that no sound is radiated from the tube :

$$u_{an} = \frac{p_{an}}{\rho_0 c} \tag{1}$$

where ρ_0 is the atmospheric density of air and c is the speed of sound in air. Typical values used in the experiments described here ranged from $p_{an} = 203\,\mathrm{Pa}$, $u_{an} = 0.49\,\mathrm{m\,s^{-1}}$ to $p_{an} = 7748\,\mathrm{Pa}$, $u_{an} = 18.67\,\mathrm{m\,s^{-1}}$.

3 Analysis

For a particular p_{an} and termination geometry, 300 image pairs are cross-correlated and filtered with a 32×32 pixel interrogation window and a 50% overlap resulting in a grid of 79×63 velocity vectors per image pair. For each phase step t_i, there are $n = 30$ instantaneous vector fields $\mathbf{u}_n(x,y,t_i)$, $n = 1 \ldots 30$. These are averaged for each phase step to give a phase-averaged vector field $\mathbf{u}(x,y,t_i)$.

3.1 POD

POD is a form of statistical analysis that has been used to identify large-scale structures in complex flows by decomposing a set of descriptive velocity fields into a basis of orthogonal eigenfunctions [4, 5, 6]. Any stage in the flow can then be reconstructed using a linear combination of these orthogonal basis modes $\mathbf{\Phi}(x,y)$ which are ordered according to kinetic energy. POD can be described as searching in the set of $\mathbf{u}(x,y,t_i)$ for the $\mathbf{\Phi}(x,y)$ which is closest on average in terms of energy to all the members in the set, then finding the orthogonal mode $\mathbf{\Phi}(x,y)$ which is next closest, etc. Mathematically this is equivalent to solving the Fredholm equation

$$\int\int \left\langle \mathbf{u}(x,y,t_i)\mathbf{u}(x',y',t_i) \right\rangle \mathbf{\Phi}_m(x',y')dx'dy' = \lambda_m \mathbf{\Phi}_m(x,y) \tag{2}$$

where λ_m is the eigenvalue corresponding to eigenfunction $\mathbf{\Phi}_m$. $\langle ... \rangle$ represents an average over time and the integrals are taken over x and y.

The experimental data obtained using PIV, having more spatial than temporal information, lends itself to the snapshot method of POD [7]. Consider a set of N_t velocity vector maps, with $N_x \times N_y$ velocity vectors in each map. The first step is to construct the correlation matrix

$$K_{ij} = \frac{1}{N_t} \sum_{x=1}^{N_x} \sum_{y=1}^{N_y} \mathbf{u}(x,y,t_i) \cdot \mathbf{u}(x,y,t_j) \tag{3}$$

where $i, j = 1 \ldots N_t$.

The eigenvectors of this matrix $V_m(t_i)$ are then found and ordered according to their eigenvalues λ_m. $V_m(t_i)$ gives the temporal evolution of each mode. λ_m is descriptive of the kinetic energy associated with each mode because the correlation matrix K_{ij} consists of terms in u^2. The corresponding spatial mode $\mathbf{\Psi}_m(x,y)$ is then calculated :

$$\mathbf{\Psi}_m(x,y) = \sum_{i=1}^{N_t} \mathbf{u}(x,y,t_i) \cdot V_m(t_i). \tag{4}$$

Any velocity map can then be described as a superposition of modes using :

$$\mathbf{u}(x,y,t_i) = \sum_{m=1}^{N_t} V_m(t_i) \mathbf{\Psi}_m(x,y). \tag{5}$$

However, $\mathbf{\Psi}_m(x,y)$ is usually normalised to $\mathbf{\Phi}_m(x,y)$ via

$$\mathbf{\Phi}_m = \frac{\mathbf{\Psi}_m}{\left(\sum_{x=1}^{N_x} \sum_{y=1}^{N_y} \mathbf{\Psi}_m \cdot \mathbf{\Psi}_m \right)^{1/2}} \tag{6}$$

and the corresponding time coefficients $a_m(t_i)$ are calculated as

$$a_m(t_i) = \sum_{x=1}^{N_x} \sum_{y=1}^{N_y} \mathbf{u}(x,y,t_i) \cdot \mathbf{\Phi}_m(x,y). \tag{7}$$

Any of the original velocity maps can then be written

$$\mathbf{u}(x,y,t_i) = \sum_{m=1}^{N_t} a_m(t_i) \mathbf{\Phi}_m(x,y). \tag{8}$$

In order to ensure that the most energetic POD mode obtained is likely to be oscillatory, the cycle-averaged flow is first subtracted from the velocity vector field at each phase step so that

$$\hat{\mathbf{u}}(x,y,t_i) = \mathbf{u}(x,y,t_i) - \tilde{\mathbf{u}}(x,y) \tag{9}$$

is analysed using POD. In the above equation

$$\tilde{\mathbf{u}}(x,y) = \frac{1}{N_t} \sum_{i=1}^{N_t} \mathbf{u}(x,y,t_i). \tag{10}$$

This is the cycle-averaged flow and describes the jet-driven acoustic streaming resulting from boundary layer separation at the termination [8]. It is common practice to remove the mean from flow velocity data before performing POD [9].

3.2 Energy transfer

λ_m (as defined in equation 2) can be used to measure the relative strength of each POD mode. Due to the way that K_{ij} is constructed (see equation 3), λ_m can be defined as

$$\begin{aligned} \lambda_m &= \frac{1}{N_t} \sum_{i=1}^{N_t} \sum_{x=1}^{N_x} \sum_{y=1}^{N_y} |a_m(t_i) \mathbf{\Phi}_m(x,y)|^2 \\ &= \frac{1}{N_t} \sum_{i=1}^{N_t} \sum_{x=1}^{N_x} \sum_{y=1}^{N_y} |\mathbf{u}_m(x,y,t_i)|^2 \end{aligned} \tag{11}$$

where

$$\mathbf{u}_m(x,y,t_i) = a_m(t_i)\mathbf{\Phi}_m(x,y) \tag{12}$$

is the velocity map described by POD mode m at time t_i. It can be seen therefore that λ_m is proportional to the kinetic energy per unit mass in POD mode m, averaged over the number of time steps.

Marx et al [2] found that the first POD mode (m = 1) approximately described the acoustic potential flow in oscillating flow around a step. In order to characterise the relative amount of energy transferred into non-linear flow effects, they defined the parameter

$$e_1 = \frac{\sum_{m=2}^{m=N_t} \lambda_m}{\sum_{m=1}^{m=N_t} \lambda_m} \tag{13}$$

which is expressed as a percentage. The difference in this study is that the cycle-averaged flow has been removed before carrying out the POD, so e_1 contains no information about the energy of the streaming.

3.3 Strouhal number

The non-dimensional number that governs when non-linear flow effects become significant is the acoustic Strouhal number, defined as

$$St_l = \frac{\omega l}{u_{an}} = \frac{l}{d_{an}} \tag{14}$$

where ω is the angular frequency of the acoustic oscillation, l is some characteristic length of the geometry where the effects are produced, u_{an} is the RMS velocity of the acoustic oscillation in the region of interest and d_{an} is the equivalent acoustic particle displacement. Generally, the criterion for the appearance of non-linear flow effects is

$$St_l < 1. \tag{15}$$

More specifically, for the case of acoustic flow in a tube, Marx et al. propose [2] :

$$St_l < 0.6. \tag{16}$$

4 Results

Figures 2, 3 and 4 show the decomposition of the flow obtained by taking the cycle average and then performing POD. These results are for the r = 0.3 mm termination at two different values of p_{an}. The upper-left vector map shows the cycle-averaged flow. The upper-right graph shows the temporal coefficients of POD modes 1 and 2, $a_1(t_i)$ and $a_2(t_i)$. The corresponding spatial fields are then given below : $\mathbf{\Phi}_1(x,y)$ on the bottom-left and $\mathbf{\Phi}_2(x,y)$ on the bottom-right.

For clarity, the vector maps show the left-hand side of the termination, with the zero of the x axis corresponding to the central axis of the tube. The vector maps have been scaled to allow comparison of the velocity magnitudes between cycle-averaged flow and the first two POD modes. Therefore, the vector map for $\mathbf{\Phi}_1(x,y)$ consists of velocity data obtained by multiplying $\mathbf{\Phi}_1(x,y)$ by the maximum value of $a_1(t_i)$. A similar process is carried out for $\mathbf{\Phi}_2(x,y)$. A reference vector is given in the top-left of each vector map.

The form of a particular POD mode at a certain time in the cycle t_i can be obtained by multiplying the vectors of the relevant vector field $\mathbf{\Phi}_m(x,y)$ by the appropriate temporal coefficient $a_m(t_i)$. We begin by examining mode 1 of the POD.

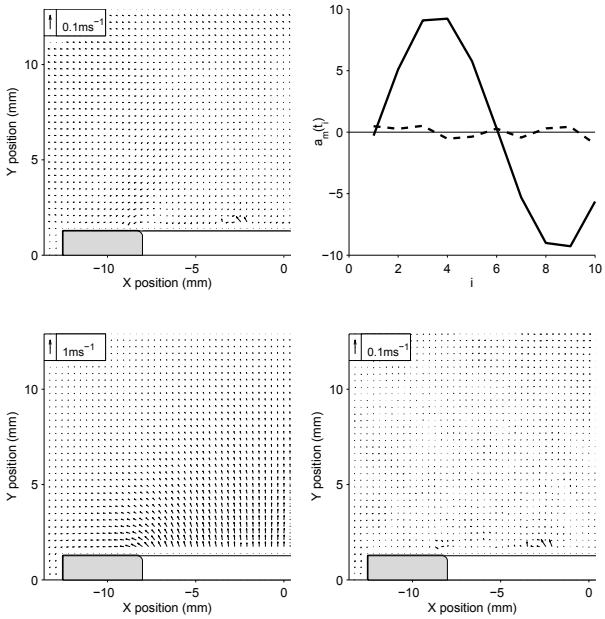

FIGURE 2 – Flow decomposition for r = 0.3 mm termination : p_{an} = 203 Pa. Top left : Streaming flow $\tilde{\mathbf{u}}(x,y)$. Top right : $a_m(t_i)$ of first 2 POD modes (**–**) a_1, (**– – –**) a_2. Bottom left : $\mathbf{\Phi}_1(x,y)$. Bottom right : $\mathbf{\Phi}_2(x,y)$. Spatial maps show left half of termination, with grey areas representing termination wall.

4.1 POD mode 1

In the case of high-amplitude oscillating flow around a step, Marx et al [2] identify the first mode of the POD with the purely acoustic motion. Three criteria are proposed here to explore the validity of this identification :

1. The coefficients $a_1(t_i)$ vary sinusoidally with time.
2. The velocity vector field $\mathbf{\Phi}_1(x,y)$ is similar in form to the $\mathbf{\Phi}_1(x,y)$ seen at low p_{an}, when non-linear flow phenomena are negligible.
3. It is possible to fully describe the non-linear flow phenomena without mode 1.

The top-right graph in figures 2 and 4 shows the time evolution of mode 1 for the two different values of p_{an}. These appear approximately sinusoidal. For p_{an} = 203 Pa (figure 2) $a_1(t_i)$ has a total harmonic distortion of 2%, calculated using the first four harmonics. The higher pressure level has a total harmonic distortion of around 10%. The pressure signal measured by the PCB transducer inside the tube typically has a total harmonic distortion of $\sim$1%, caused by the loudspeaker and any non-linear propagation.

At all values of p_{an} studied, the spatial form of the first mode of the POD ($\mathbf{\Phi}_1(x,y)$) appears roughly similar. The second criterion can be investigated in more detail by comparing the streamlines of $\mathbf{\Phi}_1(x,y)$ at low pressure level (p_{an} = 203 Pa) with those of $\mathbf{\Phi}_1(x,y)$ for higher levels. Figure 5 shows the streamline from the inside left edge of the r = 0.3mm termination at a range of p_{an}. For 203 Pa the streamline follows the geometry of the solid wall, being almost immediately parallel to the horizontal surface. As p_{an} increases the streamline increasingly deviates from the 203 Pa case. This indicates that $\mathbf{\Phi}_1(x,y)$ increasingly contains separated (non-linear) flow. A similar conclusion was made by Marx et al [2].

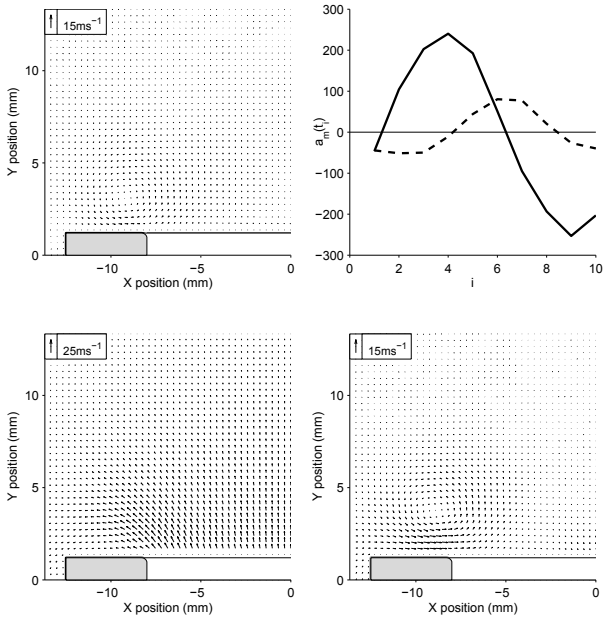

FIGURE 3 – Flow decomposition for $r = 0.3$ mm termination : $p_{an} = 5212$ Pa. Top left : Streaming flow $\tilde{\mathbf{u}}(x,y)$. Top right : $a_m(t_i)$ of first 2 POD modes (━) a_1, (━ ━ ━) a_2. Bottom left : $\mathbf{\Phi}_1(x,y)$. Bottom right : $\mathbf{\Phi}_2(x,y)$. Spatial maps show left half of termination, with grey areas representing termination wall.

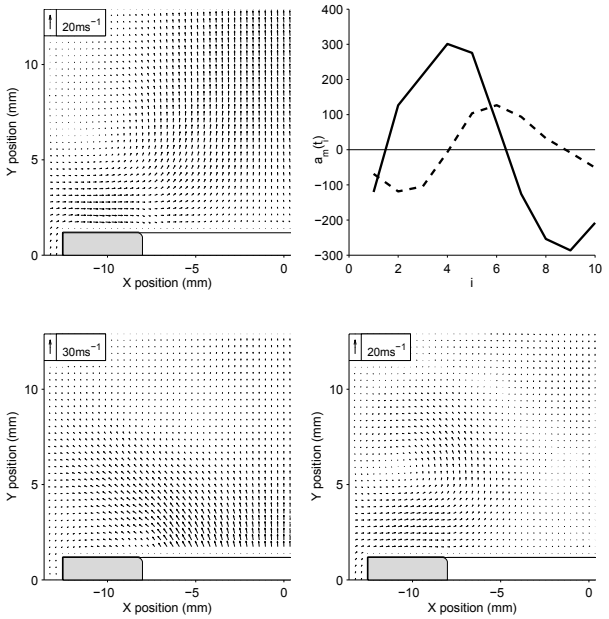

FIGURE 4 – Flow decomposition for $r = 0.3$ mm termination : $p_{an} = 7748$ Pa. Top left : Streaming flow $\tilde{\mathbf{u}}(x,y)$. Top right : $a_m(t_i)$ of first 2 POD modes (━) a_1, (━ ━ ━) a_2. Bottom left : $\mathbf{\Phi}_1(x,y)$. Bottom right : $\mathbf{\Phi}_2(x,y)$. Spatial maps show left half of termination, with grey areas representing termination wall.

To explore the third criterion we first construct

$$\mathbf{u}_{nl}(x,y,t_i) = \mathbf{u}(x,y,t_i) - a_1(t_i)\mathbf{\Phi}_1(x,y) \qquad (17)$$

which should describe the non-linear flow without the acoustic flow. We can then compare flow maps of $\mathbf{u}(x,y,t_i)$ and $\mathbf{u}_{nl}(x,y,t_i)$ at different values of p_{an} and at various points in the cycle. At lower values of p_{an} the non-linear flow features are well described by $\mathbf{u}_{nl}$. However, as the amplitude of the acoustic field increases, and especially at the two highest values of p_{an}, $\mathbf{u}$ contains flow structures that are noticeably different from those seen in $\mathbf{u}_{nl}$. This again supports the finding that the POD increasingly appropriates non-linear aspects of the flow into mode 1 at higher p_{an}. It can be seen however that $\mathbf{u}_{nl}$ approximately describes the non-linear behaviour.

4.2 Streaming and POD mode 2

Table 1 summarises the main features of $\tilde{\mathbf{u}}$, a_2 and $\mathbf{\Phi}_2$ at the different values of p_{an}. $\tilde{\mathbf{u}}$ shows three distinct regimes. From 685 Pa to 2224 Pa the streaming flow is dominated by a strong outward jet in the centre of the termination with air drawn in at the sides. 4030 Pa is a transitional level between two regimes. It features the same inward and outward flow but also the appearance of an outward rotating vortex (anti-clockwise on the left side of the termination and clockwise on the right) on the outer edge. At 5212 Pa and 5914 Pa the streaming flow becomes dominated by a strong outward vortex. A third regime is evident at 6723 Pa and 7748 Pa, where a strong central jet is evident as well as horizontal flow at the edges of the termination, flowing into the base of the jet.

The POD time coefficient of mode 2 (a_2) has a similar form at all levels, apart from the two lowest where it is indistinct. The general form is roughly sinusoidal with the positive amplitude greater than the negative. The phase is also approximately 90° behind a_1, with the maximum of a_2 occurring at the negative-going zero crossing of a_1. From 2224 Pa to 7748 Pa a_2 steadily grows in amplitude. This behaviour of a_2 is similar to that found by Marx et al. The major difference is that, in their study, a_2 never became negative. The cause of this difference is that Marx et al did not remove the cycle-averaged flow before performing POD. Therefore in their case mode 2 of the POD does not have to cancel out the cycle-averaged flow during the suction part of the cycle (see below).

The forms of $\mathbf{\Phi}_2$ at different values of p_{an} also fall into three regimes. At the two lowest pressures the flow pattern exhibits no distinguishable behaviour. From 2224 Pa onwards an outward rotating vortex at the outer edge of the tonehole is clearly visible, growing in size with increasing p_{an}. A third regime is evident at the two highest levels, where the outward rotating vortex is joined by a weaker vortex, rotating in the opposite sense and centred around position (-5,10).

To understand the evolution of the flow throughout the acoustic cycle, $\tilde{\mathbf{u}}$, a_2 and $\mathbf{\Phi}_2$ must be considered together. Taking 5212 Pa as an example (figure 3), consider phase step i = 3, when the acoustic flow is approaching the ejection maximum. $a_2(t_3)$ is then at a maximum negative value. Multiplying $\mathbf{\Phi}_2$ by $a_2(t_3)$ reverses the direction of all of the vectors. The result is an inward rotating vortex which cancels out the vortex in $\tilde{\mathbf{u}}$. The value of a_2 then increases. When a_2 becomes positive, mode 2 combines constructively with $\tilde{\mathbf{u}}$, reaching a maximum vortex strength between i = 6 and i = 7. This process describes the formation of an ejection vortex which stays attached to the end of the tube. A similar process can be applied to the flow at 7748 Pa (figure 4). Here the combination of $\tilde{\mathbf{u}}$ and mode 2 describes the formation of a strong outward jet at i = 2 and i = 3. Phase steps i = 4 to i = 8 mark the appear-

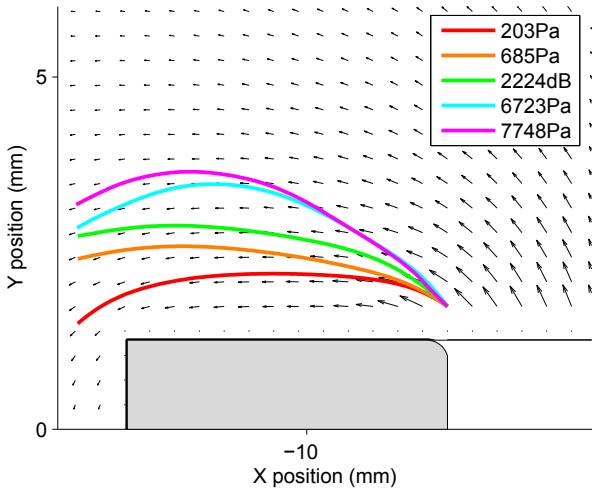

FIGURE 5 – Streamlines from the left inside edge of the r = 0.3 mm termination at a range of p_{an}. The displayed velocity field is $\Phi_1(x,y)$ for p_{an} = 203 Pa.

ance of a vortex which is separated from the end of the tube and accompanied by a counter-rotating vortex. The progression through these two regimes, vortex formation (2224 Pa to 5914 Pa) and then vortex shedding (6723 Pa and 7748 Pa), has been observed in PIV maps of the phase averaged flow $\mathbf{u}(x,y,t_i)$ [3].

4.3 Energy transfer to non-linear flow

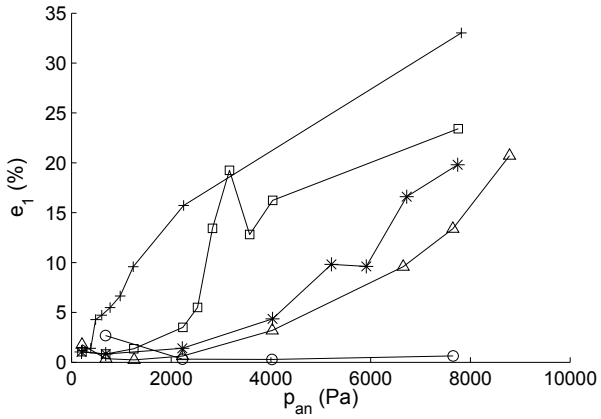

FIGURE 6 – e_1 against p_{an}. (+) r = sharp, (□) r = 0 mm, (∗) r = 0.3 mm, (△) r = 1 mm, (○) r = 4 mm.

The parameter e_1 defined in equation 13 is plotted in Figure 6 as a function of the acoustic pressure for three different terminations. The general behaviour of e_1, which represents the percentage of energy transferred into localised non-linear flow, is as expected, increasing with increasing acoustic amplitude and increasing sharpness of the inner edge of the termination. In Figure 7, e_1 is plotted against the Strouhal number obtained using the radius r as the typical length. It can be seen that the energy transfer to nonlinear flow is fairly well characterised by St_r for the examples studied. It should be recalled, however, that the cycle-averaged flow was subtracted before the POD analysis was performed, so e_1 does not include energy transferred from the linear acoustic field into

TABLE 1 – Description of non-linear flow constituents for r = 0.3 mm termination.

p_{an} (Pa)	$\tilde{\mathbf{u}}$	a_2	$\mathbf{\Phi}_2$
203	Unclear	Unclear	Unclear
685	Out at centre In at sides	Unclear	Unclear
2224	Out at centre In at sides	Oscillating 90° out of phase with a_1	Weak outward vortex
4030	Out at centre In at sides Outward vortex	Oscillating 90° out of phase with a_1	Outward vortex
5212	Strong outward vortex	Oscillating 90° out of phase with a_1	Outward vortex
5914	Strong outward vortex	Oscillating 90° out of phase with a_1	Outward vortex
6723	Strong central jet Strong side flow	Oscillating 90° out of phase with a_1	Removed outward vortex Weak inward vortex
7748	Strong central jet Strong side flow	Oscillating 90° out of phase with a_1	Removed outward vortex Weak inward vortex

streaming motion.

4.4 Streaming velocity

The significance of the cycle-averaged streaming motion can be assessed in Figure 8, which shows the streaming jet velocity u_s normalised to the acoustic particle velocity. u_s is the average streaming jet velocity calculated across a plane just above the termination, assuming a circular symmetry. In Figure 9 the normalised jet velocity is plotted against the Strouhal number. For values of $St_r \ll 1$ and $St_r \gg 1$, the streaming is well characterised by the Strouhal number; for $St_r \simeq 1$ the situation is clearly more complicated.

5 Conclusion

PIV and POD have been applied to high amplitude oscillating flow outside the end of a tube. It has been found that, when the cycle-averaged flow is first removed, mode 1 of the POD approximately describes the acoustic flow. As the sound pressure in the tube increases, more aspects of the induced non-linear flow are appropriated into mode 1. Mode 2

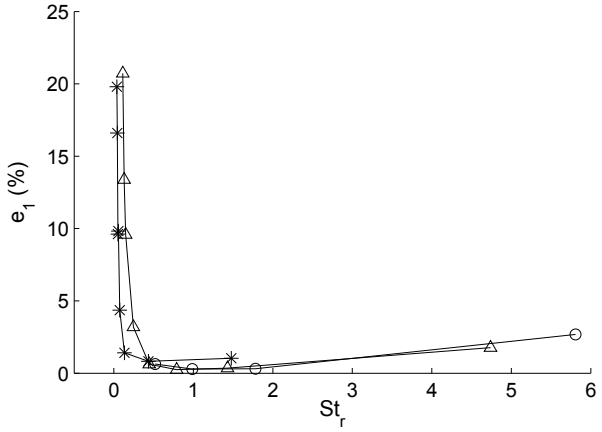

FIGURE 7 – e_1 against St_r. (∗) r = 0.3 mm, (△) r = 1 mm, (○) r = 4 mm.

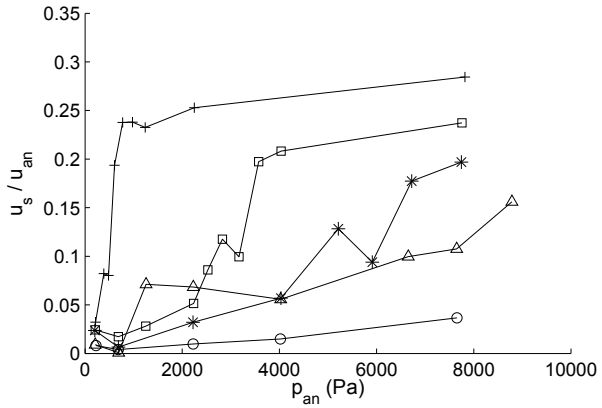

FIGURE 8 – Normalised jet velocity u_s against p_{an}. (+) r = sharp, (□) r = 0 mm, (∗) r = 0.3mm, (△) r = 1 mm, (○) r = 4 mm.

of the POD describes the formation and motion of vortices outside the tube over the course of the acoustic cycle, but must be understood together with the cycle-averaged flow to reconstruct the non-linear flow behaviour.

Once the POD analysis has been shown to approximately split the flow into acoustic and non-linear constituents, it is possible to construct the energy transfer parameter e_1. e_1 is strongly dependent on the Strouhal number of the flow.

The e_1 data for the terminations do not take into account all of the non-linear flow effects generated : energy will be required to drive the steady streaming. Also, some vortex formation and streaming will occur inside the tube [3]. It would be of interest to calculate e_1 over a region that enclosed all of the non-linear flow effects.

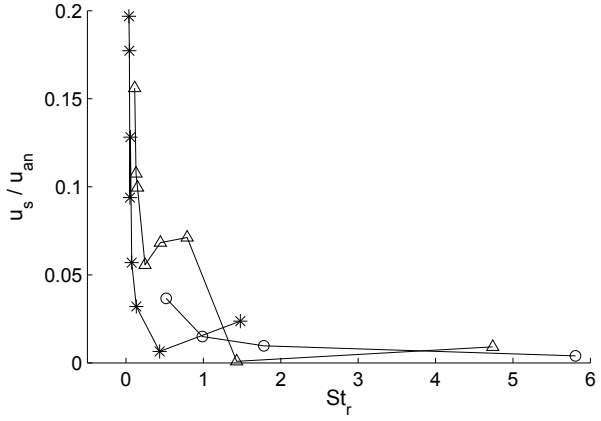

FIGURE 9 – Normalised jet velocity u_s against St_r. (∗) r = 0.3 mm, (△) r = 1 mm, (○) r = 4 mm.

Références

[1] Ingard, U., Labate, S., "Acoustic circulation effects and the nonlinear impedance of orifices", *J. Acoust. Soc. Am.* 22(2), 211-218 (1950)

[2] Marx, D., Bailliet, H., Valière, J.-C., "Analysis of the acoustic flow at an abrupt change in section of an acoustic waveguide using Particle Image Velocimetry and Proper Orthogonal Decomposition", *Acta Acustica united with Acustica* 94(1), 54-65 (2008)

[3] Skulina, D.J., "A Study of Non-linear Acoustic Flows at the Open End of a Tube using Particle Image Velocimetry", PhD thesis, University of Edinburgh (2005)

[4] Berkooz, G., Holmes, P., Lumley, J.L., "The proper orthogonal decomposition in the analysis of turbulent flows", *Ann. Rev. Fluid Mech.* 25, 539-575 (1993)

[5] Graftieaux, L., Michard, M., Grosjean N., "Combining PIV, POD and vortex identification algorithms for the study of unsteady turbulent swirling flows", *Meas. Sci. Technol.* 12, 1422-1429 (2001)

[6] Webber, G.A., Handler, R.A., Sirovich, L., "Energy dynamics in a turbulent channel flow using the Karhunen-Loéve approach", *Int. J. Numer. Meth. Fluids* 40, 1381-1400 (2002)

[7] Sirovich, L., "Turbulence and the dynamics of coherent structures, parts I-III", *Quarterly of Applied Math.* XLV, 561-582 (1987)

[8] Boluriaan, S., Morris, P.J., "Acoustic streaming : from Rayleigh to today", *International Journal of Aeroacoustics* 2, 255-292 (2003)

[9] Kostas, J., Soria, J., Chong M.S., "A comparison between snapshot POD analysis of PIV velocity and vorticity data", *Experiments in Fluids* 38, 146-160 (2005)